Holding potential affects the apparent voltage-sensitivity of sodium channel activation in crayfish giant axons

Peter C. Ruben,* John G. Starkus,* and Martin D. Rayner‡
*Békésy Laboratory of Neurobiology, Pacific Biomedical Research Center and ‡the Department of Physiology, John A. Burns School of Medicine, University of Hawaii, Honolulu, Hawaii 96822 USA

ABSTRACT Sodium channel activation, measured as the fraction of channels open to peak conductance for different test potentials ($F[V]$), shows two statistically different slopes from holding potentials more positive than −90 mV. A high valence of 4–6e is indicated at test potentials within 35 mV of the apparent threshold potential (circa −65 mV at −85 mV holding potential). However, for test potentials positive to −30 mV, the $F(V)$ curve shows a 2e valence. The $F(V)$ curve for crayfish axon sodium channels at these "depolarized" holding potentials thus closely resembles classic data obtained from other preparations at holding potentials between −80 and −60 mV. In contrast, at holding potentials more negative than −100 mV, the high slope essentially disappears and the $F(V)$ curve follows a single Boltzmann distribution with a valence of ~2e at all potentials. Neither the slope of this simple distribution nor its midpoint (−20 mV) was significantly affected by removal of fast inactivation with pronase. The change in $F(V)$ slope, when holding potential is increased from −85 to −120 mV, does not appear to be caused by the contribution of a second channel type. The simple voltage dependence of sodum current found at V_h −120 mV can be used to discriminate between models of sodium channel activation, and rules out models with three particles of equal valence.

INTRODUCTION

Hodgkin and Huxley (1952*a*) noted that normalized peak sodium conductance (g_{Na}), when plotted on a logarithmic scale, approached an asymptotic slope of 4 mV per e-fold change for small (<20 mV) depolarizations from holding potential (V_h −60 mV). Presuming that peak sodium conductance was controlled by redistribution of membrane charges according to a modified Boltzmann equation (see Hodgkin and Huxley, 1952*b*), this limiting slope was interpreted to indicate that at least six electron charges (6e) are involved in activation of the sodium channel. That estimate was reassessed by Keynes and Rojas (1976) who found the limiting slope to be 6.5 ± 0.1 mV per e-fold change in sodium conductance from V_h −60 to −100 mV, suggesting a revised valence of ~4e for the sodium channels in squid axons. Stimers et al. (1985) repeated this work using pronased axons (to avoid possible effects of fast inactivation on peak g_{Na}) and compensating for the nonlinearity of sodium channel conductance at negative potentials. They found a 7 mV per e-fold change, further confirming that ~4 charges must cross the membrane field to open each sodium channel. Holding potential was −70 mV in that study.

Address correspondence to Dr. Peter C. Ruben, University of Hawaii, Pacific Biomedical Research Center, Békésy Laboratory of Neurobiology, 1993 East West Road, Honolulu, HI 96822, Bitnet: Ruben@U Hunix.

Almers (1978) has shown that additional information may be obtained from measurements of the voltage sensitivity of sodium channels. If the logarithm of the ratio

$$\frac{Ig_{Na}}{(g_{Na_{max}} - g_{Na})}$$

is plotted against membrane potential, data points generated by a simple two-state Boltzmann system should lie along a single line. Replotting data from Hodgkin and Huxley (1952*a*), Almers demonstrated that their data did not conform to such a two-state model. Two separate slopes were apparent, suggesting a more complex multistate activation mechanism.

By contrast, the gating current data presented by Keynes and Rojas (1976) from a holding potential of −100 mV in squid axons, as well as the gating current data obtained from crayfish giant axons at strongly negative holding potentials (−140 mV) by Rayner and Starkus (1989), shows only a single slope of <2e when plotted in a similar manner. In addition, Conti and Stühmer (1989) reported a 1.8e valence for sodium gating current in rat brain II sodium channels expressed in *Xenopus* oocytes. These studies contrast with the more complex data seen at less negative holding potentials (Bezanilla and Armstrong, 1975; Armstrong, 1981; Stimers et al., 1985; Keynes, 1986). However the additional

0006-3495/90/11/1169/13 $2.00

(0.5–0.7e) slope characteristic of gating charge distributions seen under these conditions apparently results from immobilization of gating charge at holding potential (Rayner and Starkus, 1989). Thus, once the complicating effects of holding potential are more fully understood, the voltage sensitivity of the gating charges indicates a simple two-state Boltzmann process with an effective valence of $\sim 2e$.

In view of the apparent conflict between the two-state system indicated by gating current measurements and the multistate system suggested by the ionic current data, it seemed appropriate to reinvestigate the voltage sensitivity of the sodium channel from sodium current measurements. We confirm that a $>4e$ limiting slope appears in experiments where less negative holding potentials are used. However, from holding potentials more negative than -100 mV, sodium channel voltage sensitivity is well represented by a single two-state Boltzmann distribution with an effective valence of $\sim 2e$. That data is not compatible with models which assume multiple particles with identical valences.

This data has been presented in preliminary form (Ruben et al., 1989; Rayner and Ruben, 1990).

METHODS

Medial giant axons from the crayfish, *Procambarus clarkii*, were internally perfused and voltage clamped using methods adapted to crayfish axons by Shrager (1974) and further described by Starkus and Shrager (1978). Series resistance was compensated at 10 Ω-cm^2 and corrections were made for an electrode junction potential of 8–10 mV. Temperature was maintained at 6°C throughout. Our methods for data recording and for subtraction of linear capacity and leakage currents using the P/n control pulse protocols have been presented in detail by Rayner and Starkus (1989). We describe here only those additional methods required for the present study.

Measurement of peak I_{Na}

The principal errors involved in measurement of peak sodium current arise from inadequate series resistance compensation, or from the procedures used for subtraction of nonlinear leak and gating currents. Our solutions (see below) were chosen to keep peak I_{Na} to ~1.5–2 mA/cm^2 so as to minimize series resistance errors. With signal averaging of multiple pulses (up to 32 averages), the minimum current that could be accurately measured was ~1 μA/cm^2. Values beyond this range are represented by the dark gray band in Fig. 9. Time-to-peak and other measures of kinetic stability were carefully noted; we have compared records obtained at differing internal and external sodium concentrations and find no evidence indicative of inadequate compensation within this data set.

In recent studies nonlinear leak and gating currents have generally been removed by subtraction of equivalent records obtained in the presence of Tetrodotoxin. Because our experimental protocols required extended periods of data recording (usually 3–5 h) and subsequent current rundown (usually 20%; experiments with more than 50% rundown were not used for analysis) we were not able to use that method. Nonlinear leak has been minimized by appropriate internal perfusates (see below) and was measured at intervals by recording I_{Na} at the end of a 200-ms pulse to test potential. The sum of steady state I_{Na} and nonlinear leak was <10 μA/cm^2, even at 20–40 mV (<1% of total current). As pointed out by Stimers et al. (1985) the residual gating current will be negligible at peak I_{Na} in pronase-treated axons. Possible errors introduced by failure to subtract gating current from peak I_{Na} measurements in nonpronased axons are small under the experimental conditions used here: typically no more than 1% of peak I_{Na} at 20 mV and ~3% of peak I_{Na} at a test potential of -55 mV.

Solutions

Solutions (see Table 1) were adjusted to maintain peak inward sodium current at no more than ~1.5 mA/cm^2 (while minimizing both linear and nonlinear leakage currents) by mixing "high-Na" and "Na-free" solutions in appropriate proportions. Adjusted sodium concentrations are listed in figure legends as external/internal (in millimolar). Pronase used in this study was from *Streptomyces griseus* type VI or XIV (Sigma Chemical Corp., St. Louis, MO), activity: 6 proteolytic units/mg, or from Calbiochem-Behring Corp., activity: 77 proteolytic units/mg.

Computer simulations

Simulations were carried out using a Sun 3/60 computer (Sun Microsystems, El Segundo, CA). Our modeling program employs simple Euler integration to solve the array of simultaneous equations representing the allowed transitions within each particular model formulation. Cumulative errors were <0.001% at the end of each model run. All voltage steps were presumed to be instantaneous. Holding potential was set to -120 mV for each simulation and calculated initial state occupancies were used for each model run. Models were simulated in "pronased" form (i.e., without fast inactivation). For each model all transitions were specified in accordance with Eyring rate theory (Glasstone et al., 1941; Woodbury, 1971; Stimers et al., 1985) such that the rate constants $K_{a,b}$

TABLE 1 Experimental solutions

Condition	Na^+	Ca^{++}	Mg^{++}	Cs^+	Cl^-	F^-	TMA	Glutamate	Hepes	pH
200 Na Internal	200	0	0	30	0	60	0	170	1	7.35
0 Na Internal	0	0	0	230	0	60	0	170	1	7.35
210 Na External	210	13.5	2.6	0	242.2	0	0	0	2	7.55
0 Na External	0	13.5	2.6	0	242.2	0	210	0	2	7.55

Osmolarity: 430–440 mOsm.

and $K_{b,a}$ are:

$$K_{a,b} = (kT/h) \exp(-w_a - ez'\,dV/kT)$$
$$K_{b,a} = (kT/h) \exp[-w_b + ez'(1-d)V/kT],$$

where w is the height of the energy barrier (in kT units) as seen from well a or b, respectively, e is the electronic charge, z' is the effective valence of the a,b transition, d is the fraction of the distance between wells a and b at which the barrier peak occurs, V is the membrane potential, k is the Boltzmann constant, T is the absolute temperature, and h is the Planck constant. In the single model in which electrostatic coupling was introduced, this was presumed to occur only in the depolarization-favored position and to involve repulsion between two (of three) gating particles. The rate constants $K_{b,a}$ leading out of the states in which both of these particles are in their depolarization-favored positions were modified as:

$$K_{b,a} = (kT/h) \exp[-w_b + ez'(1-d)V/kT] \exp W_i,$$

where W_i is the interaction energy between particles M1 and M2. Parameters for all models (see Table 2) were generated de novo except for the Hodgkin-Huxley model for which we used their empirical equations (Hodgkin and Huxley, 1952*b*) for calculating m_∞^3 (thus presuming that inactivation had been removed using pronase). Rationale for selection of the models shown here is presented in Discussion.

Models requiring independent (or electrostatically coupled) movement of three separate particles were necessarily formulated as 8-state "cubes" similar to the 8-state models of Bezanilla et al. (1982) and Rayner and Starkus (1989). Three allosterically coupled particles can be simulated by a linear 4-state sequence; however a three particle model in which only two particles are allosterically coupled requires a 6-state "ladder" (see Alicata et al., 1990).

RESULTS

Traditional methods for calculating the fraction of open channels have assumed linearity of the instantaneous I(V) curve. Thus Hodgkin and Huxley (1952*a*) and Oxford (1981) used g_{Na}, calculated from

$$\frac{I_{Na}\text{peak}}{(V - E_{Na})},$$

to measure the fraction of open channels. However, Stimers et al. (1985) noted nonlinearity in their instantaneous I(V) curve due, in part, to the effects of calcium. Because we find similar nonlinearities in our data (see Figs. 2 *A* and 3 *A*), we conclude that the analytical procedure of Stimers et al. (1985) is more appropriate for our experimental conditions. We here describe that method in more detail.

Our experimental protocols were carefully designed to avoid artifacts induced by axon rundown. Voltage steps to test potential (for peak I_{Na} measurements) were alternated with double pulse patterns for tail current measurement at that same test potential (see Fig. 1, *pulse pattern*). Each tail current measurement required a prepulse (in most experiments +20–40 mV) before the repolarizing step to test potential, hence the prepulse peak I_{Na} provided a pulse-by-pulse control which could be used for assessing any possible rundown during the experiment. Fig. 1 shows a typical record collected by the tail-current protocol. Inactivation between the time of peak current at the prepulse potential and the start of the repolarizing voltage step (~40 μs) was corrected by scaling the linear portion of the instantaneous $I(V)$ curve to overlie the linear region of the peak $I(V)$ curve (at potentials > +10 mV). Thus, the dotted line at a' shows the value to which the peak tail current was scaled to account for inactivation during the depolarizing pre-

TABLE 2 Computer simulations

Model name	Particle	w_a	w_b	W_i	z	d	Total valence	Independent states
3 equal particles	M1	20.0	23.0	0	1.8	0.8		
	M2	20.5	23.5	0	1.8	0.2	5.4	8
No coupling (3*p*)	M3	21.7	24.7	0	1.8	0.2		
3 different particles	M1	20.0	22.6	0	1.0	0.25		
	M2	19.8	24.2	0	2.2	0.45	4.0	8
No coupling (*a*)	M3	21.8	23.2	0	0.8	0.65		
Electrostatic coupling	M1	18.0	20.6	1.0	1.0	0.5		
	M2	19.8	25.2	1.0	2.2	0.45	4.0	8
M1–M2 (*b*)	M3	21.8	23.2	0	0.8	0.65		
Allosteric coupling	M1	18.0	20.6	0	1.0	0.5		
	M2	19.8	24.2	0	2.2	0.45	4.0	6
M1–M2 (*c*)	M3	21.8	23.2	0	0.8	0.65		
Allosteric coupling	M1	20.6	22.4	0	0.8	0.7		
	M2	21.3	23.6	0	1.8	0.3	3.0	4
M1–M2–M3 (*d*)	M3	18.9	19.3	0	0.4	0.2		

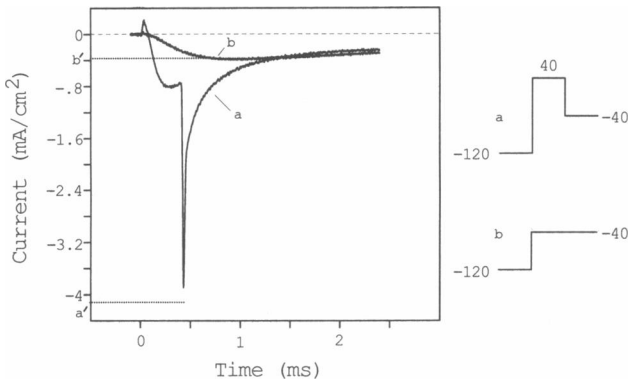

FIGURE 1 Sodium peak and tail currents are recorded to generate $I(V)_{peak}$ and $I(V)_{tail}$ curves (see Figs. 2 *A* and 3 *A*). Tail current (*trace a*) is evoked by repolarization to −40 mV after a 400-μs depolarizing step to +40 mV (*pulse pattern a*). Peak sodium current (*trace b*) is evoked by a step to −40 mV (*pulse pattern b*). Fraction of total open channels at +40 mV, which open at −40 mV (i.e., $F[-40]$), is calculated as b'/a' where b' is the amplitude of peak I_{Na} and a′ is the amplitude of tail current after correction for fast inactivation during the depolarizing prepulse (see text). Data from axon 881117 (210//0 Na).

pulse. The fraction of open channels (F) was determined at each test potential (V) by dividing the peak I_{Na} (e.g., b' in Fig. 1) by the scaled peak tail current (e.g., a' in Fig. 1).

Two statistically different slopes are apparent in $F(V)$ data when V_h is less negative than −90 mV

Fig. 2 shows the results from the application of the above protocol when holding potential was −85 mV. The instantaneous $I(V)$ curve (boxes in Fig. 2 *A*) was scaled to overlie the peak $I(V)$ curve (circles in Fig. 2 *A*), and the ratio is shown as a $F(V)$ curve in Fig. 2 *B*. When the data are linearized according to the logit method introduced by Keynes and Rojas (1974) the resulting distribution shows two distinct regions of differing slope. The slope in the range of test potential between −30 and −60 mV suggests an effective activation valence of ~5*e*, whereas the slope in the range from +30 to −30 mV suggests a valence of ~2*e* (Fig. 2 *C*). For the total of four axons in this series, the mean valence for the low slope region was 2.0*e* ± 0.1 SD whereas the higher slope seen at the more negative potentials was 4.3*e* ± 0.9 SD. These slopes are significantly different by one-way analysis of variance: $F(1,6) = 26.83$, $p = 0.002$. Thus a high limiting slope (>4*e*) can be demonstrated in crayfish axons from holding potentials similar to those used in previous studies on squid axons.

From strongly negative holding potentials, peak sodium conductance measurements conform to a single Boltzmann distribution with a slope of ~2*e* in both nonpronased and pronased axons

As noted in the Introduction, Rayner and Starkus (1989, Fig. 10) have shown that holding potential can be an important determinant of steady-state gating charge distributions. We therefore explored the possibility that the holding potentials (−60 mV, Hodgkin and Huxley, 1952*a*, *b*; −80 mV, Oxford, 1981; −70 mV, Stimers et al., 1985) used in previous studies of sodium channel voltage sensitivity may have affected the form of $F(V)$ curve, just as these holding potentials also affect the shape of the $Q(V)$ curves (Rayner and Starkus, 1989).

Fig. 3 *A* shows the curve for peak $I(V)$ (*triangles*) and the instantaneous $I(V)$ curve (*crosses*) for a typical experiment in a nonpronased axon from −120 mV holding potential. The ratio of these curves gives the fraction of open channels as a function of voltage, the $F(V)$ curve, shown in Fig. 3 *B*. Figure 3 *C* shows the composite data from eight experiments conducted from a holding potential of −120 mV. The data points have been linearized by the logit transformation and indicate a mean slope of 2.1 ± 0.2 (SD).

Neither the symmetrical shape of the $F(V)$ curve (see Fig. 4 *A*) nor the slope of the transformed data (see Fig. 4 *B*) is significantly altered when inactivation is removed with pronase. In this series of experiments the holding potential was −100 mV and ~90% of fast inactivation was removed by pronase action. Data was analyzed exactly as in the nonpronased axons, using coincident tail currents as a measure of the instantaneous $I(V)$ relationship. Effective valence in pronased axons (2.29*e* ± 0.19 SD, $n = 4$) was not significantly different from that seen in the nonpronased axons from the same data set or from the experiments described above, suggesting that fast inactivation did not appreciably contribute to the effective valence measured in these experiments.

Data from single axons confirm the effect of change in holding potential on slope of $F(V)$ curves at near-threshold test potentials

In this section we examine the effects of holding potential on ionic and gating currents from a series of axons whose longevity permitted complete data collection at two hold-

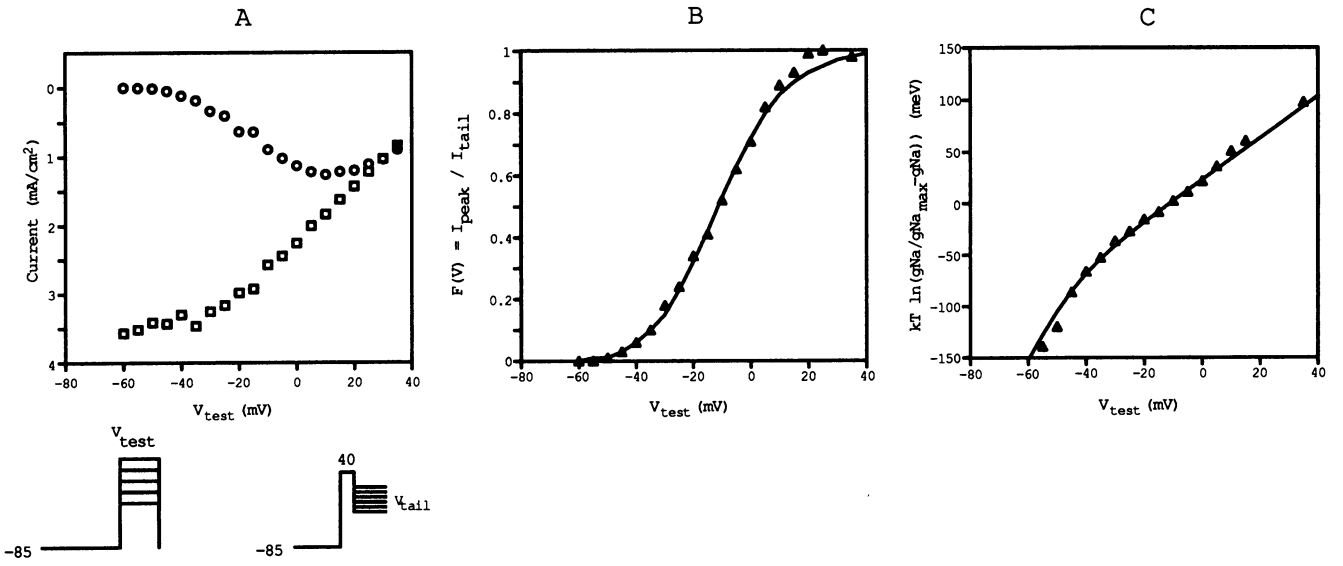

FIGURE 2 Channel activation as a function of voltage from a "depolarized" holding potential. (*A*) Peak currents (*circles*) measured during depolarization from holding potential (−85 mV) to test potential (V_{test} −60 to +35 mV) (*see left pulse pattern*) are divided by tail currents (*boxes*) evoked at the same test potential (now V_{tail}) after a 400-μs step from V_h to +40 mV (*see right pulse pattern*). The $F(V)$ distribution from this data is shown in *B* (*triangles*). (*C*) The $F(V)$ distribution is linearized by the logit transformation show two linear regions with different slopes. Lines were fit by eye to the data in *B* and *C*. Peak and tail currents from axon 881117 (210//0).

ing potentials (−85 and −120 mV). Differences in $F(V)$ curves due to these changes in holding potential can also be demonstrated in these single axons. The slopes of logit-transformed $F(V)$ curves always fell within the ranges described above.

When holding potential was −85 mV, the maximum peak I_{Na} at positive test potentials was reduced to ~55% of the current seen from a holding potential of −120 mV (see Fig. 5, *right panels*). However, where $F(V)$ curves are normalized (using coincidently measured tail currents as described above), these curves are parallel at all test potentials more positive than −30 mV. Thus the midpoint of the $F(V)$ curve is −19 mV from a holding potential of −85 mV (see Fig. 2) as compared with −21 mV from V_h −120 mV (see Fig. 3). For comparison, mid-points were −21, −28, and −11 mV for the $F(V)$ curves obtained from −120 mV, −100, and −85 mV holding potentials in Figs. 3 *B*, 4 *A*, and 2 *B*, respectively.

The relative suppression of peak I_{Na} from more depolarized holding potentials can also be seen by comparing data traces taken at different test potentials. Fig. 5 shows data traces recorded at test potentials of −60, −40, −20, and 0 mV from two holding potentials (−85 and −120 mV). The currents are shown both with the same vertical axis (*top row*) and with amplified vertical axes (*bottom row*) to emphasize the changing ratio between the peak currents evoked from the two holding potentials. Thus the ratio

$$\frac{I_{Na_{peak(-85)}}}{I_{Na_{peak(-120)}}}$$

changes with test potential from 0.04 at −60 mV to 0.19 at −40 mV and to 0.28 at −20 and 0 mV. The filled circles in Fig. 6 represent the ionic current data from Fig. 5, and show that this ratio increases linearly between −60 and −30 mV, but remains constant at ~0.30 for more positive test potentials. Thus the relative suppression seen in the current traces exactly corresponds to the region of high limiting slope seen in Fig. 2 *C*.

Near threshold, ionic current is suppressed relative to gating current by shift of V_h

We next compare these changes in I_{Na} with coincident changes in gating current (I_g) by integrating the gating currents visible in these traces over the 100-μs time period before onset of detectable inward sodium current. By contrast with the I_{Na} data the ratio of the gating charge

$$\frac{Q_{ON(-85)}}{Q_{ON(-120)}}$$

(see Fig. 6, *open circles*) does not change with test potential ($\bar{x}$ = 0.30 ± 0.05 SD shown by dashed line in

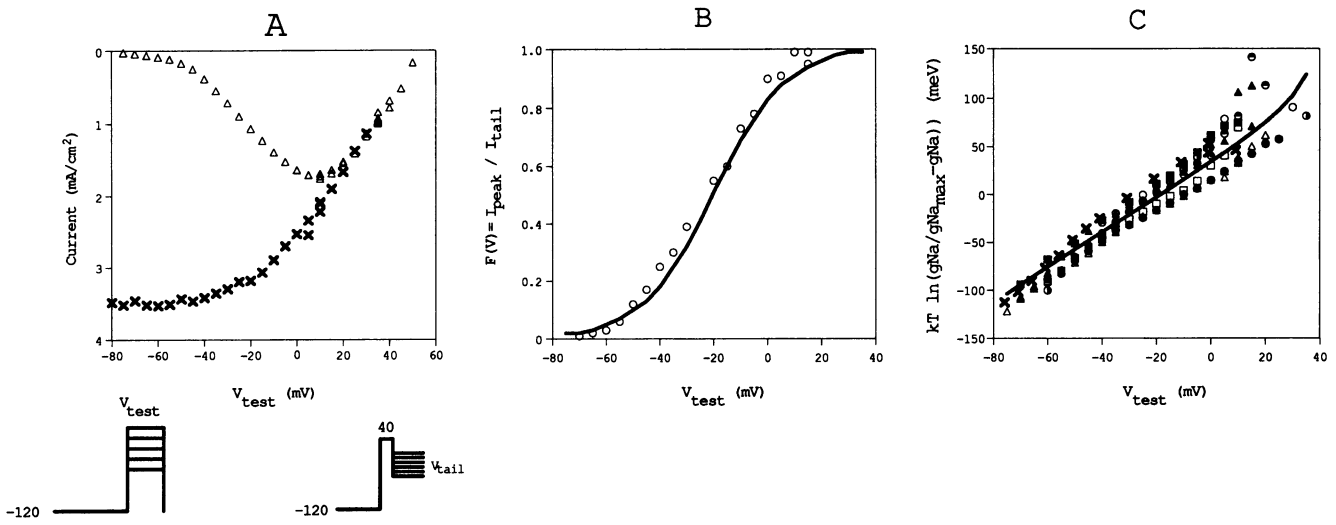

FIGURE 3 Channel activation as a function of voltage from a more hyperpolarized holding potential. (*A*) Peak currents (*triangles*) measured during depolarization from holding potential (−120 mV) to test potential (V_{test} −80 to +35 mV) (*see left pulse pattern*) are divided by tail currents (*crosses*) evoked at the same potential (now V_{tail}) after a 400-μs step from V_h to +40 mV (*see right pulse pattern*). Peak and tail currents from axon 881104b. This produces the distribution (*B*) showing the fraction of open channels as a function of test voltage (*circles*). $F(V)$ data points from axon 881026. (*C*) $F(V)$ distributions from 8 axons and fitted line from *B* are linearized by logit transformation. Average slope of the distribution suggests an average valence of ~2*e* (statistics given in text). The slight increase in slope at the positive end of the distribution is an error induced by an insufficiently positive normalization potential (+40 mV). Lines were fit to data in *B* and *C* by eye. Data from axons 881025 (105//10), 881026 (105//0), 881103 (75//5), 881031, 881104, 881104b (all 50//0), 881107b (100//0), 881117 (210//0), 900108 (52.5//0).

Fig. 6). The gating charge ratio is also constant when charge is fully integrated (to 2 ms). The constant gating charge ratio is fully consistent with the interpretation of Rayner and Starkus (1989) indicating that V_h does not affect the 2*e* slope of the $Q_{ON}(V)$ relationship. Furthermore, the I_{Na} ratio parallels the gating charge ratio at test potentials positive to −30 mV, where $F(V)$ curves of Fig. 2 and 3 are also parallel.

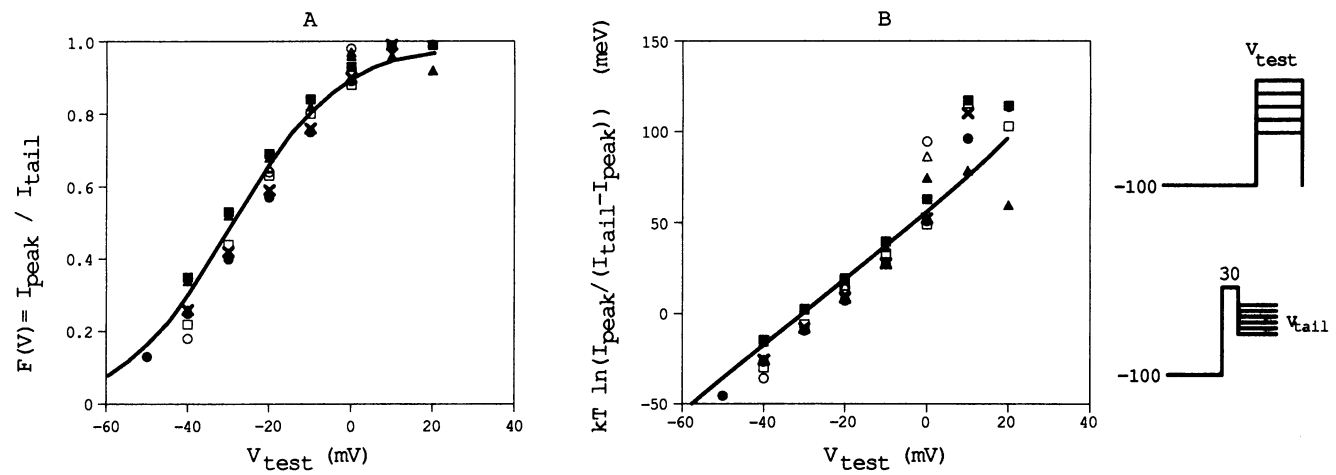

FIGURE 4 Removal of fast inactivation with Pronase does not change the fraction of open channel ($F[V]$) distribution. $F(V)$ curves were produced as in Fig. 3 (*see pulse pattern insert*). Neither the normalized data (*A*) nor the effective valence given by the average slope of linearized data points (*B*) are affected by the addition of pronase to remove fast inactivation. Lines were fit by eye to the data. Control data are shown with open symbols, Pronase data with solid symbols and crosses. Data is from axons 830321 (*squares*, 50//0 Na), 830324 (*triangles* 50//0 Na), 830616 (*circles*, 50//0 Na), and 830602 (*crosses*, 100//0 Na).

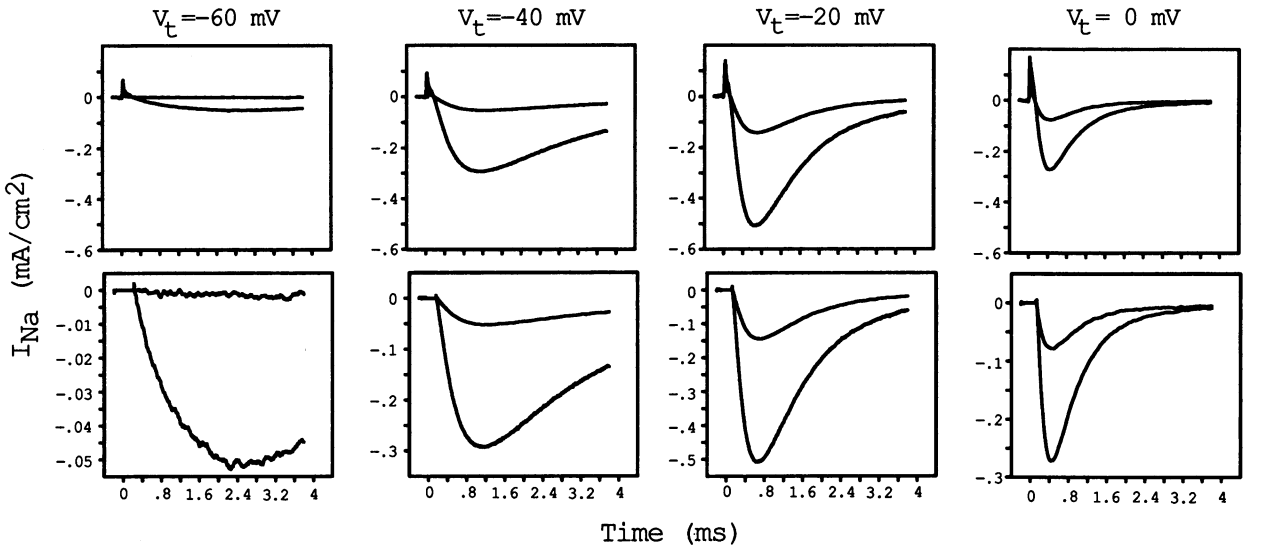

FIGURE 5 Relative suppression of sodium current from a depolarized holding potential is greater at test potentials negative to −40 mV. Top panels show unscaled gating and sodium current records evoked at V_{test} from holding potentials of −120 and −85 mV. Bottom panels show ionic currents amplified to emphasize the ratio between currents evoked from the different holding potentials; these records have had gating currents blanked for clarity. Data from axon 890727 (30//20).

I_{Na} suppression at near threshold potentials occurs without changes in activation or deactivation kinetics

Apparent suppression of ionic current could be caused by recruitment (at V_h −120 mV) and inactivation (at V_h −85 mV) of a distinct subpopulation of channels with different voltage dependence and different activation kinetics. These additional channels would sum with "normal" channels to increase sodium currents at these negative test potentials. This recruitment might well reduce the slope of the $F(V)$ curve at negative test potentials. By contrast, Fig. 7 shows that peak currents have essentially identical activation kinetics when evoked from V_h −120 and −85 mV. Smaller currents from −85 mV have been scaled to overlie the larger currents from −120 mV. In each panel, activation kinetics seem almost identical across a range of test potentials where difference in peak current magnitudes is pronounced.

On the other hand, a class of "threshold" channels with "normal" activation kinetics has been reported by Gilly and Armstrong (1984). These authors noted that a slow tail current component saturates at −40 mV test potential (V_t), and hence proposed that distinct channel populations give rise to each component of the tail current. "Threshold" channels appear to be selectively recruited at the most negative test potentials. We have therefore explored possible contributions of "threshold" channels to our results. Fig. 8 shows a family of tail currents evoked by steps to different return (V_r) potentials after a 400-μs depolarizing step to 30 mV. The return step was initiated immediately after peak I_{Na} to minimize effects of fast inactivation on tail current kinetics. Although multiple kinetics are readily visible in the tail currents, the

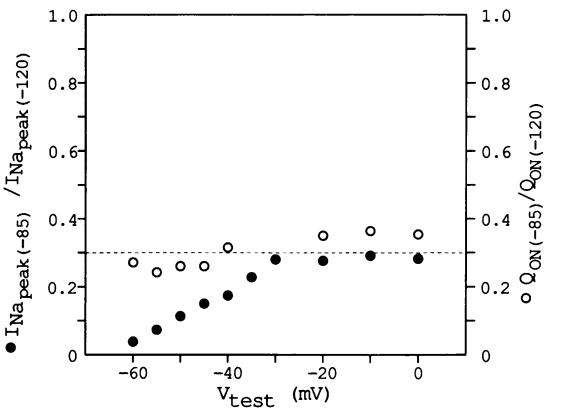

FIGURE 6 Ratio of sodium current from two holding potentials is not constant at all test potentials. Integrated gating currents (*open circles*) and peak sodium currents (*closed circles*) are plotted as the ratio of these values from −85 and −120 mV holding potentials. Relative suppression of peak sodium current from "depolarized" holding potentials is greater at test potentials more negative than −30 mV. There is no equivalent suppression in the gating currents due to changes in holding potential (mean ratio = 0.30 ± 0.05 SD shown by the dashed line). Data from axon 890727 (30//20).

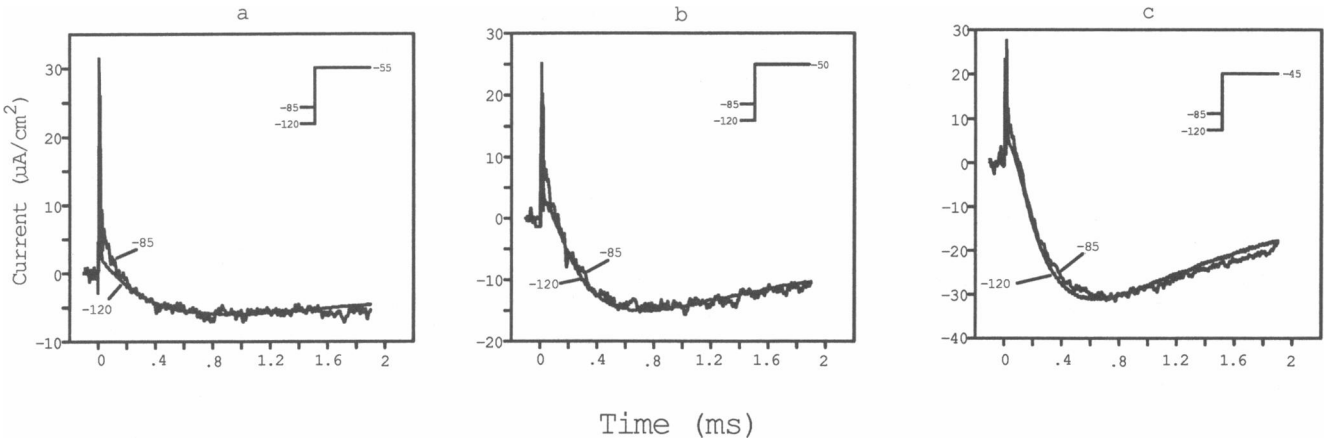

FIGURE 7 Relative suppression of sodium current is not associated with changes in activation kinetics. Currents from −120 mV holding potential have been scaled down to overlie the currents from −85 mV holding potential. Test potentials were −55, −50, and −45 mV in the *a*, *b*, and *c* panels, respectively. Data from axon 890727 (30//20).

intercept of the slow component changes with return potential. If the two kinetic components were generated by different channel populations, then the proportion of these populations should be determined only by the prior test potential and should be independent of the final return potential. This condition is clearly not met by the tail currents shown in Fig. 8 *A* and this observation seems incompatible with the "threshold" channel interpretation of tail current kinetics presented by Gilly and Armstrong (1984).

Furthermore, tail current kinetics are independent of holding potential. Selective recruitment of additional channels at hyperpolarized holding potentials should increase the slow component intercept in the tail current kinetics from V_h −120 mV. By contrast, Fig. 8 *B* shows that tail current records from V_h −120 and −85 mV scale to coincide with each other at the same return potential (−100 mV). This also seems incompatible with any "threshold" channel interpretation of our data.

DISCUSSION

The principal results of this study are: (*a*) when depolarized holding potentials (−90 to −80 mV) are used, $F(V)$ curves indicate a high limiting slope valence (as much as 4.5*e*) between threshold (−60 mV) and −30 mV. However, a lower slope of ~2*e* is visible for test potentials >−30 mV (Fig. 2 *C*). (*b*) Only the lower 2*e* valence is seen when channel voltage dependence is assessed using

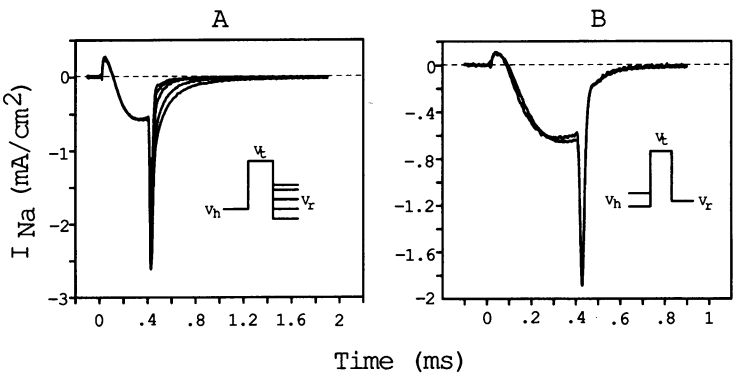

FIGURE 8 Tail current intercepts are affected by changes in return potential but not holding potential. (*A*) Tail currents were evoked at return potentials (V_r) of −70, −80, −100, −120, and −140 mV after 400 μs steps from V_h = −120 mV to a test potential (V_t) of +30 mV. The intercept of the slow component of tail current decreases with more negative return voltage. (*B*) Tail currents were evoked at return potential of −100 mV after 400 μs steps from V_h = −120 mV and V_h = −85 mV to V_t = +30 mV. Current record from V_h = −85 mV was scaled so that the maximum tail current amplitude coincided with that from V_h = −120 mV (scale factor = 1.73). Data from axon 881107b (52.5//0).

$F(V)$ curves obtained from holding potentials negative to -100 mV (Fig. 3 *C*). This effective valence estimate was not significantly changed by prior removal of fast inactivation with pronase (Fig. 4 *B*). (*c*) Ionic current is selectively suppressed for small depolarizations from more depolarized holding potentials (Fig. 5, lower panel, and Fig. 6) without an equivalent suppression of gating current (Fig. 6).

Our $F(V)$ curves from holding potentials positive to -90 mV are fully consistent with previous data from other axons at similar holding potentials. First, the data of Hodgkin and Huxley (1952*a*) from a holding potential of ~ -60 mV shows a limiting slope of 6*e* at test potentials more negative than -35 mV. However, when this data was replotted by Almers (1978, Fig. 18 *a*), a second and lesser slope is shown which can be well fitted by a 2*e* slope for all test potentials positive to -35 mV. This 2*e* slope crosses the midpoint of the total distribution of ~ -20 mV (cf. our Figs. 2 *C* and 3 *C*).

Second, Keynes and Rojas (1976, Table 3) obtained a mean of 6.5 mV per *e*-fold change in g_{Na} in the steepest region of the $g_{Na}(V)$ curve, suggesting an effective valence of 3.7*e* for the conditions of their study. Holding potentials were between -60 and -70 mV for the data reported in their table.

Third, Oxford (1981, Figs. 4 and 5) working from a holding potential of -80 mV, found a limiting slope of 5.3 mV per *e*-fold change in

$$\frac{g_{Na}}{(g_{Na_{max}} - g_{Na})},$$

This suggests an effective valence of ~4.5*e*. However the data for test potentials positive to -35 mV is again quite linear, suggesting a mean slope of ~2.8. The midpoint for the total distribution was ~ -25 mV. He obtained quantitatively similar data in pronased axons.

Fourth, Stimers et al. (1985, Fig. 4) shows $F(V)$ plots for both pronased and nonpronased axons as well as a plot of log $F(V)$ from eight pronase-treated axons. Holding potential was -70 mV in that study. Their results indicate an *e*-fold change in 7 mV suggesting a minimum activation valence of 4*e* for test potentials negative to -35 mV. However, the slope of the $F(V)$ relationship is clearly less steep at test potentials positive to -35 mV. We estimate an effective valence of ~2*e* from their data at test potentials positive to -30 mV, while the midpoint of the distribution appears to be ~ -10 mV for both the pronased and nonpronased axons shown in their Figs. 4, *A* and *B*. Finally, Gonoi and Hille (1987) have pointed out that removal of fast inactivation has no significant effect on the voltage dependence or kinetics of macroscopic sodium channel inactivation in axonal preparations.

In these studies both the midpoints of the total $F(V)$ distributions and the effective valences indicated for the low and high slope regions of the $F(V)$ curve are close to the values we have obtained in crayfish axons at similar ("depolarized") holding potentials. However, no significant high slope region appears in our data, for either pronased or nonpronased axons, when a strongly negative holding potential is used (Fig. 3 *C*). This result is confirmed by comparison of different holding potentials within a single axon as well as from data examined by a different analytical method (see Figs. 5 and 6). Nevertheless we notice a slight tendency for our $F(V)$ curves to increase in slope at test potentials more negative than -70 mV (see Fig. 3 *C*). This may indicate that a higher "limiting slope" could be resolved at V_h -120 mV by further studies concentrating on test potentials between -70 and -80 mV. We point out, however, that the difficulty of resolving any high slope region from V_h -120 mV seems quite contrary to expectations based on the ease with which the high slope can be resolved in the smaller sodium currents obtained with V_h -85 mV.

Possible mechanisms which might produce the results we have recorded fall into three general classes: (*a*) methodological errors might distort the results from V_h -120 mV, (*b*) holding potential might determine the number of particles required to open a sodium channel, (*c*) additional channel types might be recruited at very negative holding potentials, (*d*) normal channels could be selectively suppressed at more positive holding potentials. These mechanisms are considered below.

Methodological distortion of the $F(V)$ curve

Peak tail currents in crayfish axons saturate at negative return potentials but increase when extracellular calcium is reduced, indicating a voltage sensitive blockade of inward sodium currents by calcium ions similar to that seen by Yamamoto et al. (1984) in neuroblastoma cells, Stimers et al. (1985) in squid axons, and Sheets et al. (1988) in cardiac myocytes. Although our experiments could have been done at reduced $[Ca^{++}]$, this would have introduced a lateral shift in I_{Na} voltage sensitivity (Frankenhauser and Hodgkin, 1957; Hahin and Campbell, 1983) amplifying the quantitative differences between the crayfish and squid preparations. In any case, a potential-dependent calcium block would be expected to equally affect tail current amplitude and peak I_{Na} amplitude at any test potential. Similarly, calcium block is unlikely to be affected by holding potential.

Incomplete series resistance (R_s) compensation could distort the $F(V)$ curves. No R_s error was detected as kinetic shifts in I_{Na} recorded from different holding potentials (Fig. 7). Furthermore R_s error would be greatest at test potentials between -20 and $+20$ mV where

sodium currents are largest. These voltages are outside the range in which I_{Na} suppression was relieved by more negative holding potentials. In addition, the midpoints of the $F(V)$ curves are well matched from -120 and -85 mV holding potentials (Figs. 2 and 3), whereas R_s errors should be expected to shift the midpoints. Large tail currents (see Figs. 2 *A* and 3 *A*) would be more sensitive to R_s errors than the smaller peak currents. However, such errors would be expected to be greatest in the voltage region where tail currents reach a plateau, hence the effect of even a 5 mV R_s shift would not introduce significant error in our data. Furthermore, we have shown (see Fig. 5) that relative suppression of I_{Na} can be seen in the raw data (without complex data analysis).

Holding potential affects the number of particles required to open a sodium channel

Apparent changes in channel activation valence might reflect changes in the number of gating particles required to open each sodium channel. Thus one $2e$ particle might be sufficient to open a sodium channel from V_h -120 mV whereas allosteric changes within the channel molecule might require three such gating particles for channel opening from V_h -85 mV. This is perhaps the most simple explanation of the results shown in Figs. 2 and 3. However, if channel gating were controlled by the movement of a single $2e$ particle at V_h -120 mV and multiple particles are more depolarized holding potentials, then a change would be expected for monoexponential activation kinetics at V_h -120 mV to multiexponential kinetics at V_h -85 mV. However, our data (Figs. 7 and 8) show no evidence of such changes in activation kinetics.

Recruitment of an additional channel population

Differential effects of holding potential on the slope of the $F(V)$ curve could arise from differential sensitivity to V_h of two (or more) subpopulations of sodium channels. In addition to the "normal" axonal sodium channels, several sub-types have been described. Gilly and Armstrong (1984) reported "threshold" channels in squid giant axons, which show a steeper $F(V)$ curve, a more negative midpoint for this curve, as well as slower closing kinetics. Additionally, Matteson and Armstrong (1982) have noted the presence of "sleepy" channels, again in squid axons. These channels are slow to activate, very slow to inactivate, and thus are responsible for maintained "steady state" sodium currents which decay principally with the kinetics of slow inactivation. If either of these channel types were selectively recruited at V_h -120 mV, they might obscure the high limiting slope of "normal" channels seen from -85 mV. The contribution of "sleepy" channels should be evident from kinetic shifts of I_{Na}. No such shifts were detected in a comparison of activation kinetics from different V_h (Fig. 7). In addition, recruitment of "threshold" channels should result in two kinetic components in tail current records, the slower of which would saturate at test potentials more positive than -40 mV (Gilly and Armstrong, 1984). We find multiple kinetic components in crayfish tail currents (Figs. 1 and 8), and the slower component saturates with test potentials more positive than -40 mV (not shown). However the intercept of the slow components changes with different return potentials (Fig. 8 *A*). This observation is inconsistent with deactivation of two channel populations; both populations would be expected to contribute to the tail current in constant proportions across the range of return potentials. Furthermore, we find that there is no difference in tail current kinetics when assessed from different holding potentials (Fig. 8 *B*). This observation is also incompatible with the selective recruitment of "threshold" channels at V_h -120 mV. If "threshold" channels were recruited from -120 mV but became inactivated at -85 mV holding potential, then single component tail current kinetics would be expected for the more depolarized holding potential. By contrast, we observed multiple component tail currents from both holding potentials. Finally, the constant gating charge ratio

$$\frac{Q_{ON(-85)}}{Q_{ON(-120)}}$$

seen in Fig. 6 also argues against selective incorporation of an additional channel population.

An alternative explanation for multiple tail current kinetics may be that "normal" channels can close via multiple kinetic pathways. More channels close via the faster pathway when return potential is more negative; as return potential becomes less negative, an increasing proportion of channels close by way of the slow pathway.

Thus we find no evidence from our macroscopic measurements indicating recruitment of a separate, additional channel population at strongly negative holding potentials. Nevertheless, unequivocal distinction between heterogeneous channel populations and changing properties of a homogeneous population requires single channel experiments that can accurately differentiate between channel subtypes.

Holding potential-dependent changes in channel excitability

The high slope region of the $F(V)$ curve, assessed from -85 mV holding potential (Fig. 2 *C*), occurs over the same range of test potentials as the relative suppression of

peak I_{Na} seen in Fig. 6. Having dispensed with possible methodological errors and recruitment of additional channel types, we conclude that the relative suppression of peak I_{Na} is causally related to the high slope of $F(V)$ curves measured from "depolarized" holding potentials. One factor which might relate these phenomena could be slow inactivation of sodium current. A high slope region of the $F(V)$ curve is seen from -85 mV holding potential where slow inactivation is more than 50% (see Heggeness and Starkus, 1986). By contrast, no such high slope region is measured when the $F(V)$ curve is assessed from -120 mV holding potential where slow inactivation is completely removed (Heggeness and Starkus, 1986). Therefore, channel valence estimates obtained from the high slope region of $F(V)$ curves measured from depolarized holding potentials may be distorted by interaction with slow inactivation. Subsequent studies will test quantitative predictions on the nature of voltage-dependent interactions between slow inactivation and activation.

Implications for models of sodium channel activation

Although the mechanism which generates the high slope in $F(V)$ curves assessed from "depolarized" holding potentials remains largely speculative, we conclude that our data from V_h -120 mV are a valid representation of the behavior of a single, uniform channel population. We next consider the implications of this conclusion for sodium channel modeling.

The present results impose additional constraints on models of sodium channel activation. Conti and Stühmer (1989) studied *Xenopus* oocytes injected with rat brain II sodium channel mRNA. They observed gating currents with a valence of ~2*e* (see also Rayner and Starkus, 1989) and results were obtained by macroscopic fluctuation analysis indicating the presence of three gating particles. Two interpretations of Conti and Stühmer's results were proposed: (*a*) three 2*e* particles control sodium channel activation, or (*b*) only one particle has a valence of 2*e*, whereas the other particles range from ~2*e* to valences too small to be discernible by their measurement techniques. We have therefore explored a series of formulations of three particle models with equal and unequal particle valences. We find that our data from V_h -120 mV can distinguish between these two possibilities. Simulated $F(V)$ curves from one class of models that theorize independent and parallel movement of three equal-valence particles (cf. Hodgkin and Huxley, 1952; Conti and Stühmer, 1989) do not fit our experimental observations. On the other hand, another class of models with different particle valences (cf. Conti and Stühmer, 1989; Alicata et al., 1990) can be demonstrated to fit our data. Fig. 9 shows the results of these model simulations. Simulated $F(V)$ curves have been logit-transformed and plotted against the range of our experimental data from -120 mV holding potential (shown by the light gray "cloud," see Fig. 3). In Fig. 9, two curves deviate dramatically from the background of data; these are derived from the Hodgkin-Huxley model (HH) and Conti and Stühmer's model assuming three identical particles (3P). By contrast, good fits to our experimental data were obtained from all models with unequal particle valence. These models are supported by the data of Stühmer et al. (1989) who showed that site-directed mutagenesis of the S4 region in domain I had a profound effect on sodium channel activation, whereas mutagenesis of the S4 region of domain II had a much lesser effect. These results suggest unequal contribution to channel activation from the different S4 regions of the sodium channel molecule.

The unequal valence models shown in Fig. 9 were chosen to explore different levels of coupling between three charged particles: (*a*) no coupling between any of the three particles, (*b*) electrostatic coupling between two of three particles, (*c*) allosteric coupling between two of three particles, and (*d*) allosteric coupling between all three particles (see Table 2 for model parameters). Although all examples of this model class fit the present data, Alicata et al. (1990) have shown that fully-coupled

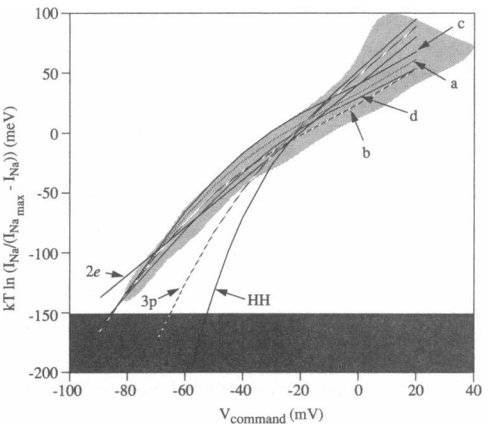

FIGURE 9 Comparison between model-generated and experimental F(V) curves. Two models with three particles of equal valence do not fit the range of data values (shown by the light gray area, see Fig 3): a Hodgkin and Huxley model (HH), and a 1.8*e* model (3p). Four models with three particles of unequal valence show close fits to the range of data values: (*a*) no coupling between particles, (*b*) allosteric coupling between two of three particles, (*c*) electrostatic coupling between two of three particles, and (*d*) coupling between all three particles. These simulated $F(V)$ curves are compared to a linearized 2*e* Boltzmann distribution (2*e*). The darker gray area represents the range over which peak I_{Na} is too small for accurate evaluation (see Methods). Holding potential was -120 mV for all model runs.

models (such as *d* in Fig. 9) are not compatible with their observation that D_20 does not effect secondary activation or Ig_{ON} kinetics. Thus the degree of coupling between particles may be of considerable importance when evaluated against other parameters of sodium channel behavior.

CONCLUSIONS

The two-state $2e$ $Q(V)$ curve has been linked by Conti and Stühmer (1989) to the multi-state $F(V)$ curve of other investigators by suggesting a system of independent particles with the same valence or with different valences. We now report that, from V_h −120 mV, the $F(V)$ curve also approximates a two-state, $2e$ Boltzmann distribution. We show, by simulating our data, that we can distinguish between Conti and Stühmer's alternative hypotheses. Three particle systems with equal valence do not fit our data from V_h −120 mV. However, multi-state systems of three particles with unequal valences can approximate simple Boltzmann distributions. We therefore conclude that such a system probably controls sodium channel activation in crayfish giant axons. In view of the significant constraints which our results place on models of the sodium channel, it seems appropriate that channel valence should also be assessed from hyperpolarized holding potentials in other preparations.

We thank Daniel Alicata for his technical assistance and Richard Foulk for assistance in programming.

This work was supported by the National Institutes of Health through both research grant NS21151-05 (to J. G. Starkus) and RCMI award 3G12RR03061-03. Additional support was received from the American Heart Association (Hawaii Affiliate), the University of Hawaii Research Council, and BRSG 2S07 RR07026 awarded by the Biomedical Research Support Grant Program, Division of Research Resources, National Institutes of Health.

Received for publication 7 August 1989 and in final form 6 July 1990.

REFERENCES

Alicata, D. A., M. D. Rayner, and J. G. Starkus. 1990. Sodium channel activation mechanisms: insights from deuterium oxide substitution. *Biophys. J.* 57:745–758.

Almers, W. 1978. Gating currents and charge movements in excitable membranes. *Rev. Physiol. Biochem. Pharmacol.* 82:6–190.

Armstrong, C. MN. 1981. Sodium channels and gating currents. *Physiol. Rev.* 61:644–683.

Bezanilla, F., and C. M. Armstrong. 1975. Properties of the sodium channel gating current. *Cold Spring Harbor Symposia in Quant. Biol.* 40:297–304.

Bezanilla, F., R. E. Taylor, and J. M. Fernandez. 1982. Distribution and kinetics of membrane dielectric polarization. I. Long-term inactivation of gating currents. *J. Gen. Physiol.* 79:21–40.

Conti, F., and W. Stühmer. 1989. Quantal charge redistributions accompanying the structural transitions of sodium channels. *Eur. Biophys. J.* 17:53–59.

Frankenhauser, B., and A. L. Hodgkin. 1957. The action of calcium on the electrical properties of squid axons. *J. Physiol.* 137:218–244.

Gilly, W. F., and C. M. Armstrong. 1984. Threshold channels—a novel type of sodium channel in squid giant axon. *Nature (Lond.).* 309:448–450.

Glasstone, S., K. J. Laidler, and H. Eyring. 1941. The Theory of Rate Processes. McGraw-Hill Inc., New York. 522–599.

Gonoi, T., and B. Hille. 1987. Gating of Na channels. Inactivation modifiers discriminate among models. *J. Gen. Physiol.* 89:253–274.

Hahin, R., and D. L. Campbell. 1983. Simple shifts in the voltage dependence of sodium channel gating caused by divalent ions. *J. Gen. Physiol.* 82:785–802.

Heggeness, S. T., and J. G. Starkus. 1986. Saxitoxin and tetrodotoxin. Electrostatic effects on sodium channel gating current in crayfish axons. *Biophys. J.* 49:629–643.

Hodgkin, A. L., and A. F. Huxley. 1952*a*. Currents carried by sodium and potassium ions through the membrane of the giant axon of *Loligo*. *J. Physiol. (Lond.).* 116:449–472.

Hodgkin, A. L., and A. F. Huxley. 1952*b*. A quantitative description of membrane current and its application to conduction and excitation in nerve. *J. Physiol. (Lond.).* 117:500–544.

Keynes, R. D. 1986. Properties of the sodium gating current in the squid axon. *In* Tetrodo-toxin, Saxitoxin and the Molecular Biology of the Sodium Channel. C. Y. Kao and S. R. Levinson, editors. *Ann. N.Y. Acad. Sci.* 479:431–438.

Keynes, R. D., and E. Rojas. 1974. Kinetics and steady state properties of the charged system controlling sodium conductance in the squid giant axon. *J. Physiol.* 239:393–434.

Keynes, R. D., and E. Rojas. 1976. The temporal and steady state relationships between activation of sodium conductance and movement of the gating particles in the squid giant axon. *J. Physiol. (Lond.).* 255:157–189.

Matteson, D. R., and C. M. Armstrong. 1982. Evidence for a population of sleepy sodium channels in squid axon at low temperature. *J. Gen. Physiol.* 79:739–758.

Oxford, G. S. 1981. Some kinetic and steady-state properties of sodium channels after removal of inactivation. *J. Gen. Physiol.* 77:1–22.

Rayner, M. D., and J. G. Starkus. 1989. The steady state distribution of gating charge in crayfish giant axons. *Biophys. J.* 55:1–19.

Rayner, M. D., and P. C. Ruben. 1990. The voltage sensitivity of sodium channel activation in crayfish axons. *Biophys. J.* 57:298*a*. (Abstr.)

Ruben, P. C., J. G. Starkus, and M. D. Rayner. 1989. Sodium channel activation in crayfish giant axons: 1. Measurement of channel valence from sodium current. *Biophys. J.* 55:404*a*. (Abstr.)

Sheets, M. F., D. A. Hanck, and H. A. Fozzard. 1988. Divalent block of sodium current in single canine cardiac purkinje cells. *Biophys. J.* 53:535*a*. (Abstr.)

Shrager, P. 1974. Ionic conductance changes in voltaged clamped crayfish axons at low pH. *J. Gen. Physiol.* 64:666–690.

Starkus, J. G., and P. Shrager. 1978. Modification of slow sodium inactivation in nerve after internal perfusion with trypsin. *Am. J. Physiol.* 4:C238–244.

Stimers, J. R., F. Bezanilla, and R. E. Taylor. 1985. Sodium channel activation in the squid giant axon. Steady state properties. *J. Gen. Physiol.* 85:65–82.

Stühmer, W., F. Conti, H. Suzuki, X. Wang, M. Noda, N. Yahagi, H. Kubo, and S. Numa. 1989. Structural parts involved in activation and inactivation of the sodium channel. *Nature (Lond.).* 339:597–603.

Woodbury, J. W. 1971. Eyring rate theory model of the current-voltage relationships of ion channels in excitable membranes. *In* Chemical Dynamics: Papers in Honor of Henry Eyring. J. O. Hirschfelder, editor. John Wiley & Sons, New York. 601–617.

Yamamoto, D., J. Z. Yeh, and T. Narahashi. 1984. Voltage-dependent calcium block of normal and tetramethrin-modified single sodium channels. *Biophys. J.* 45:337–344.